JACS
JOURNAL OF THE AMERICAN CHEMICAL SOCIETY

ARTICLE

pubs.acs.org/JACS

Interstaple Dithiol Cross-Linking in $Au_{25}(SR)_{18}$ Nanomolecules: A Combined Mass Spectrometric and Computational Study

Vijay Reddy Jupally,[‡] Rajesh Kota,[‡,§] Eric Van Dornshuld,[‡,§] Daniell L. Mattern,[‡] Gregory S. Tschumper,[‡] De-en Jiang,[†] and Amala Dass*[,‡]

[†]Chemical Sciences Division, Oak Ridge National Laboratory, Oak Ridge, Tennessee 37831, United States

[‡]Department of Chemistry and Biochemistry, University of Mississippi, University, Mississippi 38677, United States

Supporting Information

ABSTRACT: A systematic study of cross-linking chemistry of the $Au_{25}(SR)_{18}$ nanomolecule by dithiols of varying chain length, HS−$(CH_2)_n$−SH where n = 2, 3, 4, 5, and 6, is presented here. Monothiolated Au_{25} has six [RSAuSRAuSR] staple motifs on its surface, and MALDI mass spectrometry data of the ligand exchanged clusters show that propane (C3) and butane (C4) dithiols have ideal chain lengths for interstaple cross-linking and that up to six C3 or C4 dithiols can be facilely exchanged onto the cluster surface. Propanedithiol predominately exchanges with two monothiols at a time, making cross-linking bridges, while butanedithiol can exchange with either one or two monothiols at a time. The extent of cross-linking can be controlled by the $Au_{25}(SR)_{18}$ to dithiol ratio, the reaction time of ligand exchange, or the addition of a hydrophobic tail to the dithiol. MALDI MS suggests that during ethane (C2) dithiol exchange, two ethanedithiols become connected by a disulfide bond; this result is supported by density functional theory (DFT) prediction of the optimal chain length for the intrastaple coupling. Both optical absorption spectroscopy and DFT computations show that the electronic structure of the Au_{25} nanomolecule retains its main features after exchange of up to eight monothiol ligands.

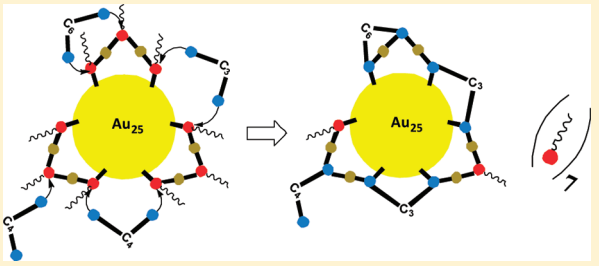

INTRODUCTION

Metal and semiconducting nanoparticles[1−3] have been widely used in medicine,[4] bioanalysis,[5] drug delivery,[6] catalysis,[7,8] and other applications.[9] Thiolated gold nanoclusters,[10] especially ultrasmall gold nanomolecules[11] (<2 nm), have garnered tremendous interest[12−14] due to their size-dependent electrochemical[12,15,16] and optical properties.[17,18] Among the various core sizes, $Au_{25}(SR)_{18}$ is shown to be extremely stable,[19] and the R group has been varied to produce both water-soluble[19] and organic-solvent-soluble clusters.[20−25] $Au_{25}(SCH_2CH_2Ph)_{18}$ (simply referred to as Au_{25}) is the most-studied cluster due to its solubility in CH_3CN[20,26] and relative ease of isolation from the nanocluster mixture.

Self-assembled monolayers (SAMs) are well-defined molecular assemblies that have reproducible properties.[27,28] Thiolated Au nanoclusters can be viewed as three-dimensional analogues of SAMs or of surface layers on nanoparticles.[27,29] In other words, well-defined nanoclusters such as $Au_{25}(SR)_{18}$ can be used as a model for studying Au surface chemistry. Au_{25}, because of its relative low mass of ∼7 kDa, is easily amenable to mass measurements in commercially available mass spectrometers. Thus, the highly stable, easily synthesized, and readily MS-characterized Au_{25} nanoclusters can be used to study the surface chemistry by mass measurements.

Gold nanoparticles are being used increasingly in biological applications that require chemical stability, solubility in buffer solutions, and stability under extreme conditions such as strongly acidic or basic buffers. Surface passivation of Au nanoparticles by multidentate thiol binding is shown to improve the colloidal stability.[30−39] Poly(ethylene glycol) (PEGylated) multidentate ligands have been used to impart water solubility and minimize nonspecific interactions.[40]

Previous reports have documented the synthesis of gold nanoclusters protected by dithiols.[35,41,42] Aromatic dithiol exchanges on Au_{25} have been reported previously, and resultant nanoclusters are shown to lose the distinct Au_{25} electronic transitions.[43] The exchange of a chiral aromatic dithiol, binapthyldithiol (BINAS), on Au_{38} nanoclusters has been reported recently.[44] Ligand exchange has been used to introduce new functionality while the core size of the nanocluster is preserved.[45−48]

Ultrasmall nanoclusters such as $Au_{25}(SR)_{18}$ are nanomolecules that have precise number of core gold atoms and organic passivating ligands. What is unique about Au_{25} is its high-symmetry centered icosahedral core with six RS−Au−SR−Au−SR motifs (also referred to as the semiring or long staple or staple dimer motif; here we simply call it the staple motif). The stereochemistry of these six motifs makes exchange of bidentate-binding dithiols on Au_{25} very interesting, inviting many unanswered questions. For example, what is the optimal carbon chain length between the bidentate thiol groups to have the most ready

Received: July 11, 2011
Published: November 22, 2011

Scheme 1. Synthesis of *N*-(1,3-Dimercaptopropan-2-yl)hexadecanamide (5)[a]

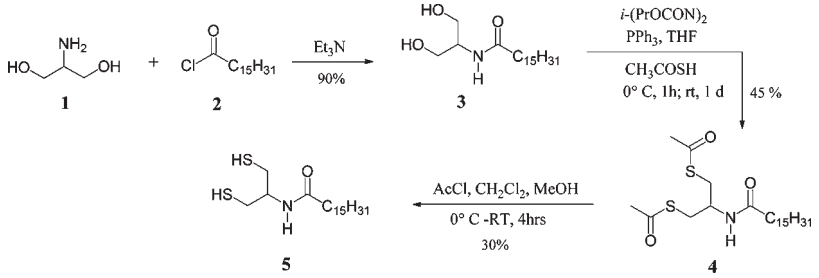

[a] Spectral data: ^{1}H NMR (300 MHz) (MeOD) δ 0.91 (t, 3H), 1.30 (m, 26H), 1.62 (m, 2H), 2.2 (t, 2H), 3.6(d, 4H), 3.9 (q, 1H).^{13}C NMR (300 MHz) (MeOD) δ 14.6.0, 23.93, 26.9, 30.5, 30.6, 30.8, 30.9, 32.9, 37.3, 54.5, 61.9, 175.1.

exchange reaction? Are both of the thiol groups anchored on the gold core? Do dithiols favor inter- or intrastaple binding? Does the bidentate binding affect the electronic structure of the nanocluster? To answer these questions, we used a series of bidentate thiols of increasing linker length from C2 to C6 to probe the ligand exchange chemistry of Au_{25} by employing mass spectrometry, UV−vis spectroscopy, and first-principles electronic structure computation.

EXPERIMENTAL METHODS

Chemicals. The following chemicals were used:1,2-Ethanedithiol (Pfaltz & Bauer, 95%), 1,3-propanedithiol (Aldrich, 99%), 1,4-butanedithiol (Aldrich, 99%), 1,5-pentanedithiol (Aldrich, 96%), 1,6-hexanedithiol (Aldrich, 96%), phenylethanemercaptan (SAFC, ≥99%), sodium borohydride (Aldrich, ≥99%), tetraoctylammonium bromide (TOABr) (Acros, 98%), *trans*-2-[3-(4-*tert*-butylphenyl)-2-methyl-2-propenylidene]malononitrile (DCTB matrix) (Fluka, ≥99%). Solvents toluene, methanol, dichloromethane, acetonitrile, and acetone were used from Fisher as received.

Equipment. UV−visible absorption spectra were recorded in toluene on a Shimadzu UV-1601 instrument. Matrix-assisted laser desorption time-of-flight mass spectra were collected on a Bruker Autoflex mass spectrometer in linear positive mode using a nitrogen laser (337 nm) with DCTB as a matrix.

Synthesis of $Au_{25}(SCH_2CH_2Ph)_{18}$. $HAuCl_4 \cdot 3H_2O$, dissolved in water, was added to dichloromethane along with the phase transfer agent TOABr. The mixture was stirred for 30 min at 500 rpm. The excess water was removed from the reaction, and 2-phenylethanethiol (3 equiv with respect to the Au salt) was added. The reaction was stirred for 30 min until the solution turned colorless. Then a solution of sodium borohydride (ca. 12 mol or 48 equiv with respect to the Au salt) in ice-cold water was added to the reaction mixture. The whole reaction was maintained at 0° for 1 h. Excess sodium borohydride was removed by washing several times with water, and excess thiol was removed by washing with methanol. Pure $Au_{25}(SCH_2CH_2Ph)_{18}$ was separated using solvent fractionation.

Ligand Exchange Reaction. $Au_{25}(SCH_2CH_2Ph)_{18}$ (0.50 mg, 68 nmol) was dissolved in 0.5 mL of toluene. To this was added the appropriate amount of dithiol corresponding to the specified ratio. The stirring rate used was 500 rpm. Samples were collected at different time intervals during the course of the reaction. The samples were concentrated by rotary evaporation and washed repeatedly with methanol until there was no smell of thiol in the sample. After further rotary evaporation and dissolution in toluene, MALDI spectra were recorded from a DCTB matrix.

To avoid confusion in the nanocluster to dithiol ratio, here we use the notation 18:*x*, where 18 represents the number of monothiol ligands present in the starting nanocluster, and *x* represents the equivalents of dithiol added per starting nanocluster. For example, 18:180 indicates that for every 18 starting ligands, 180 dithiol molecules were added for the ligand exchange.

Note that ligand exchange of sufficiently long and flexible dithiols (C4 and longer chains) may lead to cross-linking of multiple nanoclusters, resulting in an insoluble material. The concentration of the Au_{25} nanoclusters and excess dithiols are optimized to minimize this cross-linking.

Synthesis of *N*-(1,3-Dihydroxypropan-2-yl)hexadecanamide (3). 2-Aminopropane-1,3-diol (2.00 g, 22.0 mmol) and triethylamine (2.26 g, 22.4 mmol) were dissolved in 250 mL of methanol, and the mixture was cooled to −20 °C (Scheme 1). Then, 6.61 g (24.2 mmol) of palmitoyl chloride in 20 mL of THF was slowly added with stirring. The reaction mixture was stirred for another 3 h at −20 °C and then overnight at room temperature. The C16-serinol compound **3** precipitated and was collected by filtration, washed with methanol, and crystallized from 95% EtOH, giving 6.52 g (90% yield) of white crystals, mp 124.5−125.5 °C (lit.[49] 125−125.5 °C).

Synthesis of *S*,*S*′-(2-Hexadecanamidopropane-1,3-diyl) Diethanethioate (4). Diisopropyl azodicarboxylate (1.06 mL, 4.75 mmol) was added dropwise to a stirred solution of PPh_3 (1.24 g, 4.74 mmol) in THF (2 mL) at 0 °C under nitrogen. After 5 h, a solution of diol **3** (500 mg, 1.58 mmol) and thioacetic acid (603 mg, 7.92 mmol) in THF (1 mL) was added. The reaction mixture was stirred at 0 °C for 1 h and then at room temperature for 1 day. After dilution with AcOEt (100 mL), the reaction mixture was washed with saturated $NaHCO_3$ (aq), water, and saturated NaCl (aq), dried over $MgSO_4$, and concentrated in vacuum. The residue was purified by silica gel chromatography with hexane:EtOAc (100:10−50) to give dithioacetate **4** (310 mg, 45%) as a white crystalline solid, mp 85.5−86 (R_f = 0.50, hexane:ethyl acetate 1:1). ^{1}H NMR (500 MHz) ($CDCl_3$) δ 0.9 (t, 3H), 1.28 (m, 26H), 1.58 (m, 2H), 2.1 (t, 2H), 2.3 (s, 6H), 3.06−3.18 (d x d, 4H), 4.21 (m, 1H), 5.8 (d, 1H). ^{13}C NMR (500 MHz) ($CDCl_3$) δ 14.11, 22.69, 25.61, 29.21, 29.35, 29.50, 29,63, 29.66, 29.69, 30.53, 31.92, 32.17, 36.74, 36.78, 50.09, 50.17, 173.14, 196.20.

Synthesis of *N*-(1,3-Dimercaptopropan-2-yl)hexadecanamide (5). Deprotection of dithioacetate **4** was accomplished by dropwise addition of 2 mL of acetyl chloride to a solution of **4** (100 mg, 0.232 mmol) in 10 mL of dry DCM and 2 mL of dry MeOH at 0 °C. The reaction mixture was stirred at room temperature overnight. The solvent was removed under reduced pressure, and the residue was dissolved in DCM, washed twice with 20 mL of 5% $NaHCO_3$, dried over $MgSO_4$, and concentrated in vacuum. The residue was purified by silica gel chromatography with hexane: ethyl acetate (100:10−40) to yield **5** (20 mg, 30%) as a white solid (R_f = 0.50, hexane:ethyl acetate 1:1). This compound was used for the ligand exchange reaction immediately. ^{1}H NMR (300 MHz) ($CDCl_3$) δ 0.87 (t, 3H), 1.27 (m, 26H), 1.57−1.64 (m+s, 2H + H_2O), 2.22 (t, 3H), 2.71 (m, 2 H), 2.94 (m, 2H), 4.20 (q, 1H), 5.7 (d, 1H). ^{13}C NMR (300 MHz) ($CDCl_3$) δ 14.15, 22.71, 25.74,

dx.doi.org/10.1021/ja206436x |*J. Am. Chem. Soc.* 2011, 133, 20258–20266

26.75, 29.28, 29.35, 29.37, 29.50, 29.67, 29.70, 31.93, 36.87, 51.16, 172.85.

COMPUTATIONAL METHODS

Conformations of gas-phase dithiols HS−$(CH_2)_n$−SH (n = 2−5) were explored at the B3LYP[50−52]/6-311+G**[53,54] level of theory as implemented in the Gaussian09[55] quantum software package. Initial structures were generated by systematically sampling the torsional space of the C and S backbone. Full geometry optimizations were performed for all unique permutations of τ(X−C−C−Y) torsional angles (where X, Y = C or S) corresponding to syn (0°), gauche (±60°), and anti (180°) rotamers. An analysis of the intrastaple S−S distances in the Au_{25} XRD crystal structure as well as the interstaple first-, second-, and third-nearest neighbor S−S distances revealed four target R(S−S) range distances potentially suitable for dithiol bridges.

For dithiol conformations with an optimal S−S distance close to or within the target ranges, a series of relaxed scans were performed to examine how the electronic energy changed as R(S−S) increased or decreased. In other words, all other geometrical parameters were optimized for a series of fixed S−S distances spanning the appropriate range.

The structure and energetics of Au_{25} after dithiol exchange were computed using Turbomole V6.0 for parallel resolution-of-identity density functional theory (RI-DFT) calculations.[56] The nonempirical Tao−Perdew−Staroverov−Scuseria (TPSS)[57] form of meta-generalized gradient approximation (meta-GGA) was used for electron exchange and correlation, because it has been shown[58] that the TPSS functional can describe the aurophilic interactions in gold clusters and gold complexes better than the local density approximation (LDA), GGA, and hybrid functionals. The def2-SV(P) orbital and auxiliary basis sets[59] were used for all atoms for structural optimization. Effective core potentials which have 19 valence electrons and include scalar relativistic corrections were used for Au.[60] The force convergence criterion was set at 1.0×10^{-3} a.u.

RESULTS AND DISCUSSION

The XRD crystal structure[61,62] of the $Au_{25}(SCH_2CH_2Ph)_{18}$ nanomolecule shows the presence of 13 Au atoms in the core protected by six [RS−Au−SR−Au−SR] staple entities. It is easily synthesized, stable in air and most common laboratory conditions, possesses distinct UV−vis features, and displays a unique HOMO−LUMO gap and a molecular mass of ∼7400 Da, making it amenable to characterization in commercially available mass spectrometers. Here we have chosen Au_{25} as a model system to probe the surface chemistry and interactions of dithiols with the Au surface. Because the changes to Au_{25} can be measured by a change in mass by mass spectroscopy, we can obtain concrete information on the surface chemistry, which in the past has had to rely on expensive and time-consuming instrumentation such as Auger, XAFES, etc.

Exchange with 1,3-Propanedithiol. Figure 1 shows the MALDI MS of the $Au_{25}(SCH_2CH_2Ph)_{18}$ nanomolecule after ligand exchange with 1,3-propanedithiol. The masses m of the $SCH_2CH_2CH_2S$ and SCH_2CH_2Ph groups are 106 and 137 Da, respectively. If a single dithiol exchanges with one monothiol, denoted as 1D→1, then the difference in mass, Δm, is −30 Da. If a single dithiol exchanges with two monothiols, denoted as 1D→2, then Δm is −168 Da. The green peak marked by 0 is the original nanoparticle with no exchanges. The red peaks marked by 1, 2, 3, 4, 5, and 6 appear at successive Δm's of −168 and hence correspond to a series of 1D→2 exchanges, where one dithiol bridges the positions formerly occupied by two monothiols.

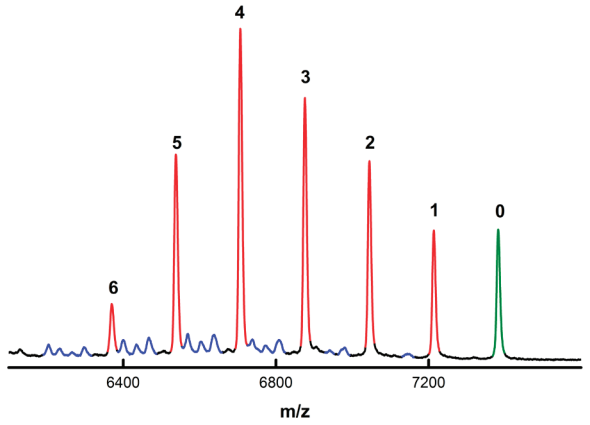

Figure 1. MALDI MS of $Au_{25}(SCH_2CH_2Ph)_{18}$ ligand exchanged with 1,3-propanedithiol. The green peak corresponds to original $Au_{25}(SCH_2CH_2Ph)_{18}$ with no exchanges. The red peaks correspond to one dithiol exchanging with two monothiols (1D→2). The numbers denote the number of such exchanges. The remaining low intensity peaks could not be assigned but are expected to arise from multiple 1D→1 exchanges. The ratio of original nanocluster ligand to incoming thiol used is 18:1800.

Exchange with 1,4-Butanedithiol. Ligand exchange data for butanedithiol are shown in Figure 2. The mass, m, of the $SCH_2CH_2CH_2CH_2S$ and SCH_2CH_2Ph groups are 120 and 137 Da, respectively. The Δm's for 1D→1 and 1D →2 are −16 and −154 Da, respectively. Red peaks denoted by 2, 3, 4, 5, 6, and 7 differ by multiples of −154 Da from the mass of the original Au_{25}, corresponding to 1D→2 exchanges. While the red peaks are the most intense, a substantial fraction of blue peaks are also present that correspond to multiple 1D→1 exchanges. This is in contrast to propanedithiol, where only a very minor fraction of smaller peaks appear and those only at higher exchanges. Figure 2b shows that the maximum number of total exchanges (including 1D→1 and 1D→2) proceeds up to 15 peaks, leaving only 3 unexchanged phenylethyl thiolate ligands.

Exchange with 1,5-Pentanedithiol and 1,6-Hexanedithiol. Figure 3 shows the ligand exchange data for $Au_{25}(SCH_2CH_2Ph)_{18}$ with 1,5-pentanedithiol and 1,6-hexanedithiol. Both the C5 and C6 dithiols show clear 1D→2 exchanges, with Δm of −140 and −126 Da, respectively. Possible 1D→1 exchanges with C5 and C6 would lead to Δm's of −2 and +12 Da, respectively, but these could not be observed because of limitations in the instrumental resolution.

Effect of Dithiol Ratio. Next, we investigated the effect of the nanomolecule to dithiol ratio on the extent of ligand exchange. The ratio is denoted by the 18:x notation, where for every 18 starting ligand groups, x molecules of dithol are added. The mole ratios of 18:18, 18:180, 18:1800, and 18:5000 were studied as shown in Figure 4. The extent of exchange was proportional to the ratio used, so that the number of exchanges and distribution of exchanges were controllable. Nanomolecules with mainly one exchange were obtained with the 18:18 ratio. Ratios of 18:180 and 18:1800 led to a broader distribution of exchanges, and the 18:5000 ratio pushed the ligand exchanges to mainly three, four, and five exchanges. Further exchanges are possible but could not be observed in MALDI because of solubility issues.

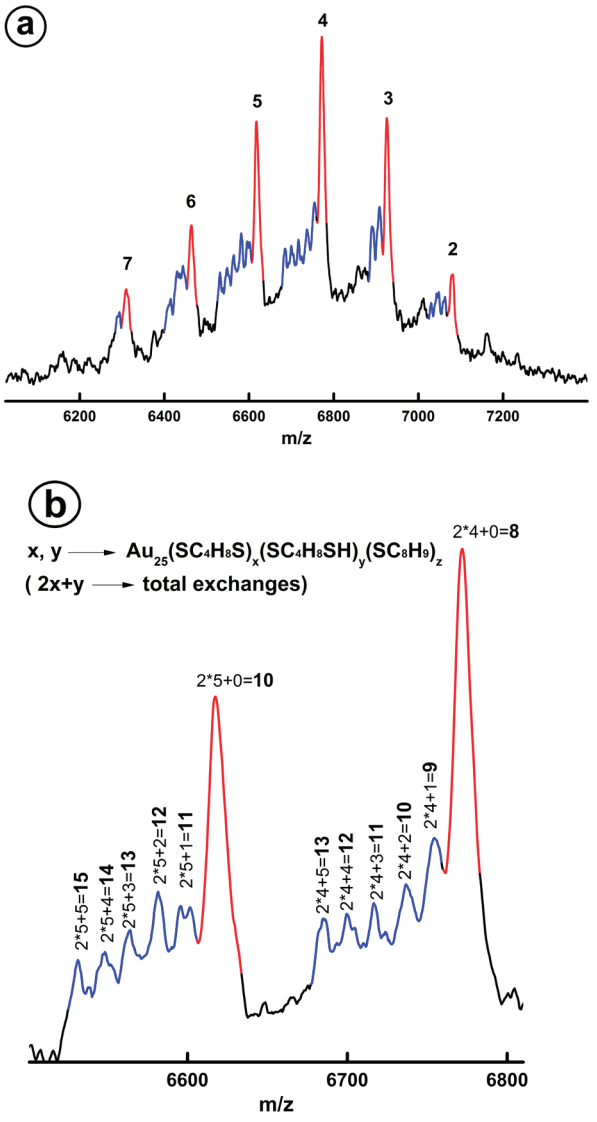

Figure 2. (A) MALDI MS of $Au_{25}(SCH_2CH_2Ph)_{18}$ ligand exchanged with 1,4-butanedithiol. The red peaks correspond to one dithiol exchanging with two monothiols; the number indicates the number of such dithiol exchanges. The blue peaks correspond to one dithiol exchanging with one monothiol. The ratio of original nanocluster ligand to incoming thiol used is 18:1800. (B) Expanded view of 4 and 5 peaks that shows number of 1D⟶2 and 1D⟶1 peaks in each set of peaks. The total number of exchanges are also denoted and proceed up to 15.

Time Evolution of Exchange. The extent and number of ligand exchanges were also studied as a function of reaction time. Figure 5 shows the progression of ligand exchange with 1,4-butanedithiol with time. As noted earlier in Figure 2, the C4 data showed many 1D⟶1 peaks in addition to the more-prominent 1D⟶2 peaks. Figure 5 shows that the number of 1D⟶1 peaks increases with time.

Intrastaple versus Interstaple Dithiol Binding. The experimental results of dithiol exchange above prompts the question of how exactly a dithiol(ate) replaces two monothiolates of the RS−Au−SR−Au−SR staple motifs on the surface of the Au_{25} cluster. Because we know the structure of the Au_{25} cluster already, this question can be addressed through electronic-structure computational techniques. One unique feature of the staple motif is

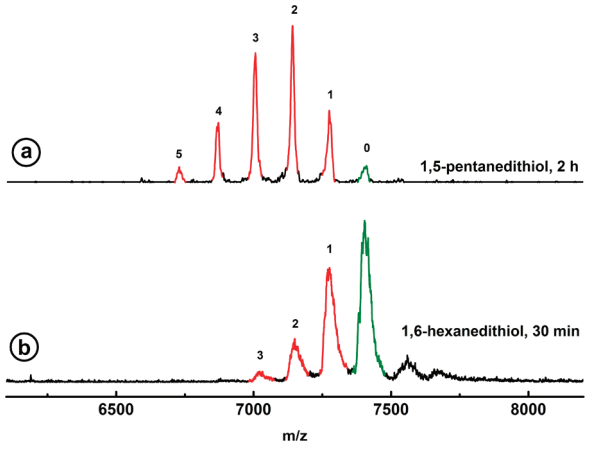

Figure 3. MALDI MS data for $Au_{25}(SCH_2CH_2Ph)_{18}$ exchanged with (a) 1,5-pentanedithiol, or (b) 1,6-hexanedithiol. The green peak corresponds to original unexchanged $Au_{25}(SCH_2CH_2Ph)_{18}$. The red peaks correspond to one dithiol exchanging with two monothiols; the number indicates the number of such dithiol exchanges. The ratio of original nanocluster ligand to incoming thiol used is 18:1800.

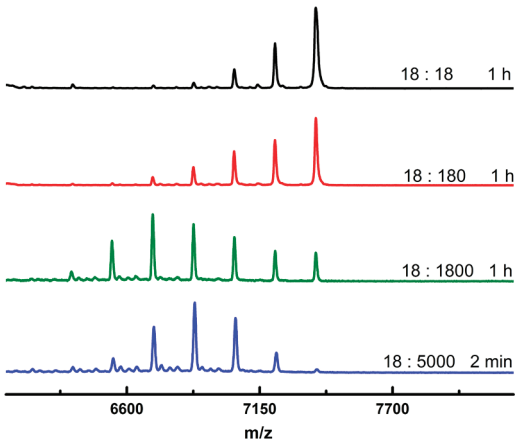

Figure 4. Steady-state product of $Au_{25}(SCH_2CH_2Ph)_{18}$ ligand exchanged with 1,3-propanedithiol as a function of the ratio of starting nanocluster to dithiol.

the linear S−Au−S bond, which is a thermodynamically favored bonding mode.[63] Therefore, an intrastaple coupling would be likely if it could maintain the roughly linear S−Au−S bond. This question can be addressed by examining the anion complex between 1,*n*-dithiolate and Au(I) as shown in Scheme 2 and by asking at what linker length *n* a linear S−Au−S bond is best achieved; Figure 6 plots the S−Au−S angles in the optimized geometries of the anion complexes. One can see that once the linker length reaches six (i.e., for 1,6-dithiolate), the S−Au−S angle is roughly linear (171°), and a nearly linear angle (179°) can be achieved for 1,8-dithiolate. The angle for 1,7-dithiolate is in between (176°). For 1,2-dithiolate the S−Au−S bond is substantially strained. In fact, intrastaple coupling is unlikely for 1,2-dithiol to 1,5-dithiol; these dithiols may prefer interstaple coupling. Moreover, 1,6-, 1,7-, and 1,8-dithiols are good candidates for intrastaple coupling.

We have performed a direct computational comparison of intrastaple versus interstaple coupling for 1,4-dithiols and 1,5-dithiols.

dx.doi.org/10.1021/ja206436x |*J. Am. Chem. Soc.* 2011, 133, 20258–20266

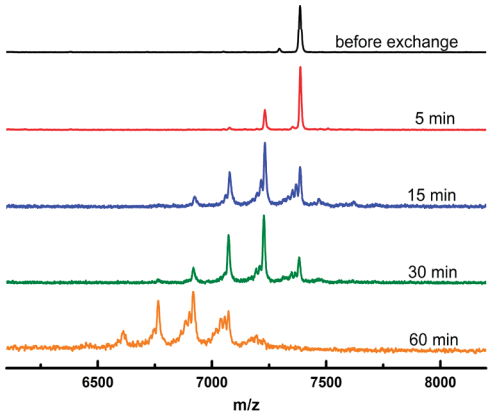

Figure 5. MALDI data of $Au_{25}(SCH_2CH_2Ph)_{18}$ ligand exchanged with 1,4-butanedithiol as a function of time.

Scheme 2. Au(I) Binds to a Dithiolate Ligand: What Linker Length (n) Best Maintains the Linear S−Au−S Bond?

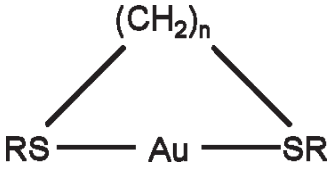

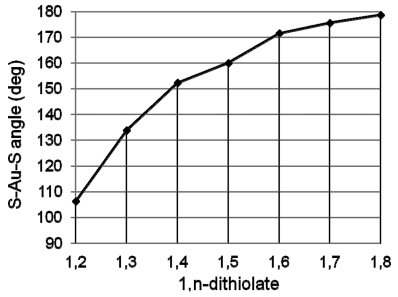

Figure 6. S−Au−S angle in the optimized structure of the anion complex between Au(I) and 1,n-dithiolate (see Scheme 2 for the structure).

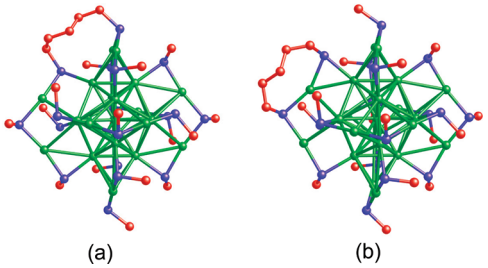

Figure 7. $Au_{25}(SCH_3)_{16}$(1,5-pentanedithiolate): (a) interstaple coupling versus (b) intrastaple coupling. Interstaple coupling is 9 kcal/mol more stable than intrastaple coupling. Au, green; S, blue; C, red; H, not shown.

Using $Au_{25}(SCH_3)_{18}^-$ as the parent cluster, we found that the exchange product $Au_{25}(SCH_3)_{16}$(1,5-pentanedithiolate)$^-$ is 9 kcal/mol more stable in the interstaple mode (Figure 7a) than in the intrastaple mode (Figure 7b). For 1,4-dithiol exchange, the interstaple mode is even more stable, by 18 kcal/mol. This computational comparison clearly shows that the interstaple coupling is favored compared to intrastaple coupling for 1,5- or shorter dithiols.

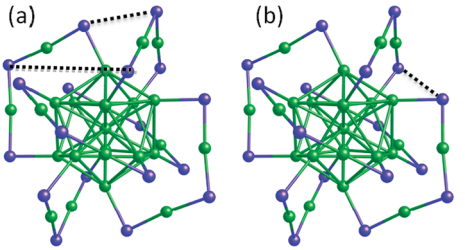

Figure 8. Proposed mode of interstaple coupling by a dithiol: (a) middle-terminal coupling (upper dashed line) and long-range middle-terminal couping (lower dashed line); (b) terminal−terminal coupling (2nd nearest neighbor). (Au, green; S, blue; C and H, not shown).

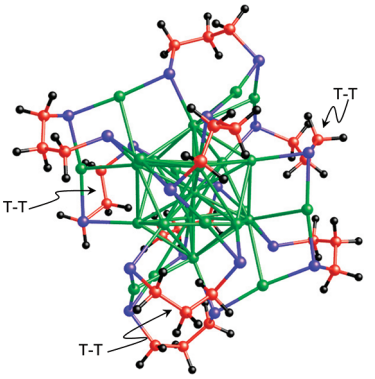

Figure 9. DFT-optimized structure Au_{25}(1,3-propanedithiolate)$_9^-$. The three dithiolates with the terminal−terminal coupling mode (T-T) are highlighted; the rest are with the middle-terminal mode. Au, green; S, blue; C, red; H, black.

Interstaple coupling for short dithiols can explain why six exchanges are easily achieved in the case of 1,3-dithiol or 1,4-dithiol. The reason is that the 18 monothiolates on Au_{25} can be divided into two groups: six in the middle of each staple that are farther from the Au_{13} core, and 12 at the terminals of the six RS−Au−SR−Au−SR motifs. We propose that the preferred exchange for small dithiolates happens between the middle thiolate of one staple and one terminal thiolate of a neighboring staple (shown by the upper dashed line in Figure 8a). We call this interstaple coupling the "middle-terminal" mode. The middle-terminal mode is analogous to the first nearest neighbor definition introduced earlier for S−S distances and discussed further below. There is another long-range variant of this mode that corresponds to third nearest neighbor in the crystal structure (shown by the lower dashed line in Figure 8a). The six middle thiolates should yield six facile middle-terminal couplings, as observed in the case of 1,3- and 1,4-dithiols. After six middle-terminal exchanges, then terminal−terminal coupling (shown by the dashed line in Figure 8b) can happen, which is analogous to the second nearest neighbor.

Is a Complete Dithiol Exchange (9 dithiols exchanging 18 monothiols) Possible in Au_{25}? In principle, one can achieve the full nine exchanges, i.e., six middle-terminal couplings and three terminal-terminal couplings. Figure 9 shows a DFT-optimized

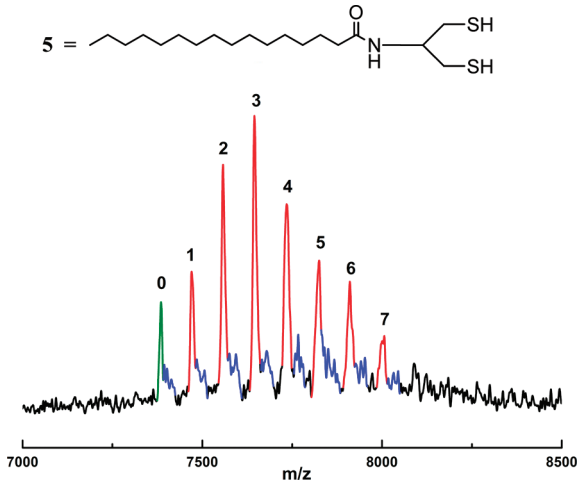

Figure 10. MALDI MS data of $Au_{25}(SCH_2CH_2Ph)_{18}$ ligand exchanged with **5**, a propanedithiol attached to a C15 chain through an amide group. The green peak corresponds to original unexchanged $Au_{25}(SCH_2CH_2Ph)_{18}$. The red peaks correspond to one dithiol exchanging with two monothiols; the number indicates the number of such dithiol exchanges. The blue peaks correspond to one dithiol exchanging with one monothiol.

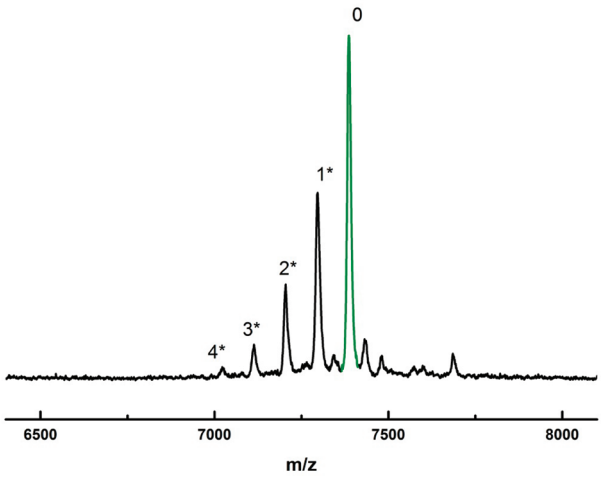

Figure 11. MALDI MS data of $Au_{25}(SCH_2CH_2Ph)_{18}$ ligand exchanged with 1,2-ethanedithiol. The green peak corresponds to original $Au_{25}(SCH_2CH_2Ph)_{18}$ with no exchanges. In solution, two molecules of 1,2-ethanedithiol combine to form a disulfide ($HS-CH_2-CH_2-S-S-CH_2-CH_2-SH$). Peak 1* corresponds to one such disulfide replacing two monothiols. The numbers on the peaks correspond to the number of disulfides replacing two monothiols each. Please refer to Scheme 3. The peaks that are heavier than original Au_{25} are unidentified.

structure of a fully exchanged Au_{25} cluster with nine 1,3-ditholates. The overall geometry of the Au_{25} cluster is well maintained; the electronic structure (frontier orbitals and HOMO−LUMO gap) is also almost unchanged from the $Au_{25}(SCH_3)_{18}^-$ (data not shown). Of course, under the experimental conditions, the probability of exchange will decrease significantly after six changes, as some terminal thiolates may be left too far apart to be coupled after six middle-terminal exchanges. However, if the exchange process is reversible and dynamic, we assume that the cluster will try to lower its energy by achieving the most stable configuration and degree of exchange. In the case of 1,4-dithiol, seven exchanges occur (Figure 2a) but not in the case of 1,3-dithiol (Figure 1). Figure 9 indicates that, in principle, more than six exchanges can be achieved for 1,3-dithiol.

In an earlier work on chiral and rigid aromatic dithiol (binapthyldithiol, BINAS) exchange on Au_{38} and Au_{40} nanoclusters, we suggest an intrastaple binding.[44] It is important to note the differences between the two systems: (a) The current work utilizes Au_{25}, which has six identical long [SR−Au−SR−Au−SR] staples, while the earlier work with Au_{38} has a mixture of short [SR−Au−SR] and long staples, (b) the current work employs flexible aliphatic ligands of variable chain length while the earlier work utilizes rigid aromatic ligands. In the previous work, we proposed that the BINAS ligand exchanges with the sulfurs in the short staple only.

To achieve more than six exchanges for 1,3-dithiol, we employed the "like dissolves like" principle to increase the likeness between the monothiolate and the dithiol(ate), to facilitate the exchange. We synthesized **5**, an analogue of the C3 dithiol with a C15 chain tethered by an amide group (Scheme 1). When a 1,3-propanedithiol replaces two phenylethanethiols, 16 carbon atoms are replaced by 3. When five or six such exchanges occur, solubility is dramatically lowered. When **5** replaces two phenylethanethiols, 16 carbon atoms are replaced by 19, leaving the solubility of the nanocluster product relatively unaffected. Figure 10 shows the MALDI data of $Au_{25}(SCH_2CH_2Ph)_{18}$ exchanged with **5**. The intense peaks in the spectra correspond to 1D→2 exchange with a Δm of +222 Da. This pattern, with a series of 1D→2 predominant peaks, agrees well with that of the 1,3-propanedithiol data (Figure 1). More importantly, we see a significant increase in six and seven exchanges and a minor peak for eight exchanges using the C15 analogue.

Scheme 3. 1,2-Ethanedithiol Forming Disulfide before Undergoing Ligand Exchange with $Au_{25}(SCH_2CH_2Ph)_{18}$

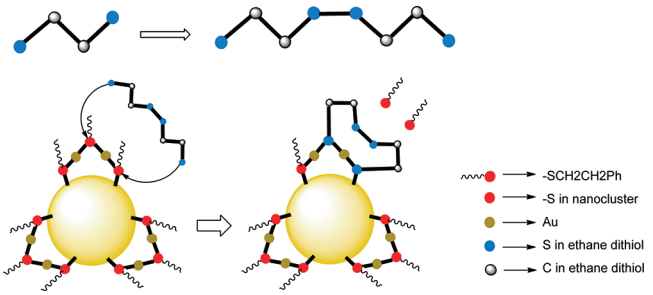

Ligand Exchange of $Au_{25}(SCH_2CH_2Ph)_{18}$ with 1,2-Ethanedithiol. The MS (Figure 11) does not show peaks that correspond to either 1D→1 (Δm −44) or 1D→2 (Δm −182). However, the peaks match with exchange of the disulfide dimer of ethanedithiol as shown in Scheme 3 (Δm −90). We propose an intrastaple coupling mode because this agrees well with our prediction that 1,6-dithiol or longer can have intrastaple coupling (Figure 6), and the disulfide bond makes this ligand resemble a 1,6-dithiol. Although we show the disulfide forming before exchange in Scheme 3, it is also conceivable that two 1D→1 exchanges occur first, followed by oxidative coupling of the dangling thiolates to make the disufide bridge.

Sulfur−Sulfur Distances. The ranges of first-, second-, and third-nearest neighbor interstaple S−S distances in the crystal structure of Au_{25} are denoted in Figure 12 by arrows at

dx.doi.org/10.1021/ja206436x |J. Am. Chem. Soc. 2011, 133, 20258–20266

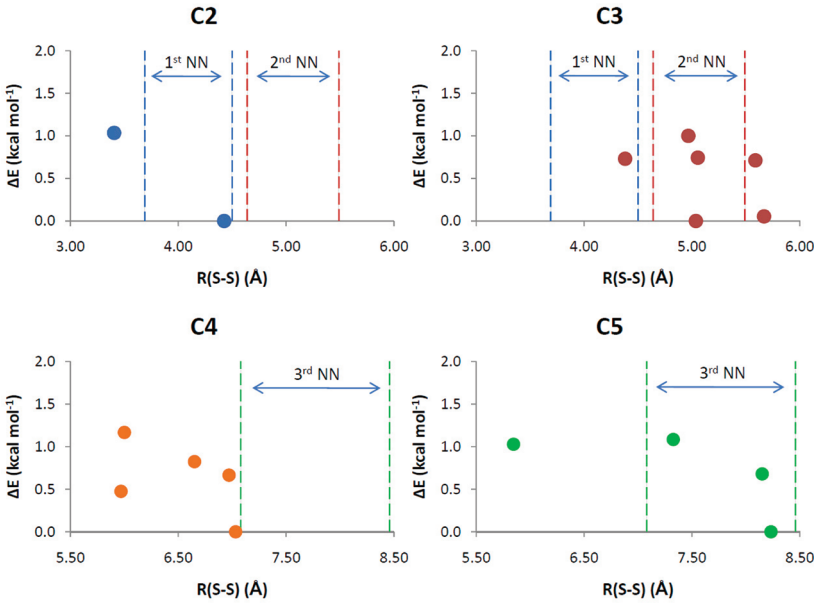

Figure 12. Relative energies (ΔE) and interstaple S−S distances, R(S−S), of the low energy conformers of C2, C3, C4, and C5, where the 1st, 2nd, and 3rd nearest neighbor (NN) ranges are indicated by the arrows.

3.69−4.50 Å, 4.64−5.49 Å, and 7.08−8.46 Å, respectively. The intrastaple target range is located at 4.61−4.65 Å. These target ranges allow the prediction of which dithiols are candidates to make dithiol bridges on Au_{25} staples. The length of dithiols needed to bridge third-nearest neighbors is likely underestimated because of steric interactions from nearby atoms spatially prohibiting a direct dithiol bridge linkage.

The effect of the S−S distance on the gas-phase dithiol conformer energy shows which conformers are candidates for forming interstaple and intrastaple bridges in Au_{25}. The target energy for a likely bridge candidate is within 2 kcal mol^{-1} of its global minimum.

One C2 conformer (Figure 12) has a minimum within the first nearest neighbor target range of 3.69−4.50 Å, suggesting candidacy for nearest-neighbor S−S bridging. However, this particular conformer has a torsional angle τ(S−C−C−S) of approximately 180°, which means the two carbons would encroach on the intervening Au atom even though the S−S separation is favorable. Another low-energy conformation can be found near R(S−S) = 3.41 Å. This structure has a more favorable τ(S−C−C−S) of 65° for interstaple alignment, but placing the S atoms at the closest target distance of 3.69 Å increases the energy by about 2 kcal mol^{-1}.

Several low-energy C3 conformers (Figure 12) have multiple S−S separations that fall within the first- and second-nearest neighbor ranges of 3.69−4.50 Å and 4.64−5.49 Å as well as the intrastaple target range of 4.61−4.65 Å. The energies of all sampled conformations rapidly increase for larger values of R(S−S), and it appears that propanedithiol is too short to bridge the third-nearest neighbor sulfurs. Several low-energy C4 conformers (Figure 12) have S−S separations that fall within the second nearest neighbor range of 4.64−5.49 Å [not shown in Figure 12] as well as the intrastaple target range of 4.61−4.65 Å. The energies of the C4 conformers rapidly increase for smaller and larger values of R(S−S) suggesting that they are not good candidates for first or third nearest neighbor bridging. Several low-energy C5 conformers have multiple S−S separations that align well with the target range for interstaple bridging between third nearest neighbors. These computational results are consistent with the lack of experimental evidence for dithiol bridging in C2.

Effect of Dithiol Exchange on the Electronic Structure of Au_{25}. We investigated if the cross-linking of two staple moieties by dithiols affects the electronic structure of the Au_{25} nanomolecules. To this end, aliquots of samples were obtained over time and purified to remove dithiols. The optical spectra of these processed dithiol exchanged aliquots were recorded, and then mass spectra were obtained, as shown in Figure 13. First, we note that the optical density of the processed Au_{25} nanoclusters decreased with time, suggesting loss of soluble material. The decrease in concentration of soluble Au_{25} is likely due to multiple reasons: (a) internanocluster cross-linking may lead to insoluble oligo/polymers, (b) Au_{25} nanoclusters stirred for longer durations (several hours) in the presence of excess thiol may convert to Au(I) thiolate species, (c) purification of sample aliquots to remove excess thiol before optical measurements will lead to some loss of Au_{25}.

Second, and more importantly, we note that the fine spectral features of Au_{25} are not affected significantly even after one, two, and three exchanges have occurred with 1,4-butanedithiol. In other words, despite the decrease in optical density, *the electronic features of Au_{25} are preserved even after dithiol exchange*. This contradicts an earlier report where the ligand exchange of Au_{25} with toluene-3,4-dithiol results in a complete loss of electronic features.[43] The aromatic dithiol employed in the earlier work is much more rigid compared to the series of aliphatic dithiols, specifically the 1,4-butanedithiol used in Figure 13 here. It would appear that the rigidity of the dithiol may play a role in how the electronic structure is affected by ligand exchange. However, it is more likely that the Au_{25} ligand exchange with aromatic thiols (unpublished results) leads to decomposition of the Au_{25} nanoclusters, as suggested in the earlier report.[43]

To corroborate our UV−vis results, we calculated the electronic-structure change as the number of exchanges of 1,4-butanedithiol on the Au_{25} cluster increased. The unexchanged $Au_{25}(SCH_3)_{18}^-$ cluster has a HOMO−LUMO gap of 1.36 eV,

dx.doi.org/10.1021/ja206436x |J. Am. Chem. Soc. 2011, 133, 20258–20266

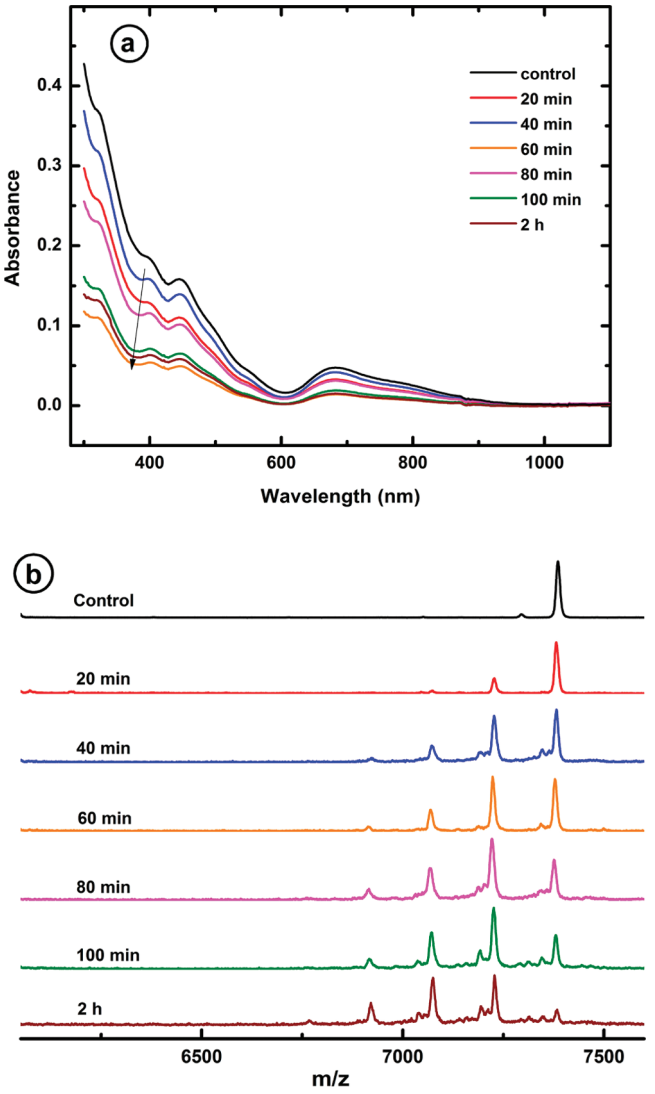

Figure 13. Changes in (a) UV−vis electronic transitions of $Au_{25}(SCH_2CH_2Ph)_{18}$ in toluene as a function of ligand exchange with 1,4-butanedithiol, as shown by (b) MALDI MS data. The starting ligand to dithiol ratio was 18:1800. Aliquots of the reaction mixture were purified to remove excess thiol before UV−vis and MALDI measurements were made.

Table 1. HOMO−LUMO Gap for 1,4-Butanedithiol-(BDT)-Exchanged $Au_{25}(SCH_3)_{18}^-$ and Energy Levels of Frontier Orbitals-(all in eV)

cluster	HOMO−LUMO gap	HOMO levels	LUMO levels
$Au_{25}(SCH_3)_{18}^-$	1.36	−2.12, −2.10, −2.08	−0.72, −0.69
$Au_{25}(SCH_3)_{16}(BDT)_1^-$	1.35	−2.12, −2.09, −2.09	−0.73, −0.70
$Au_{25}(SCH_3)_{14}(BDT)_2^-$	1.31	−2.12, −2.09, −2.07	−0.76, −0.70
$Au_{25}(SCH_3)_{12}(BDT)_3^-$	1.31	−2.11, −2.10, −2.06	−0.75, −0.72
$Au_{25}(SCH_3)_{10}(BDT)_4^-$	1.30	−2.12, −2.10, −2.07	−0.77, −0.73

together with roughly triply degenerate HOMOs and doubly degenerate LUMOs. With an increasing number of 1,4-butanedithiol exchanges for SCH_3, there is a slow narrowing of the HOMO−LUMO gap and slight perturbations of the HOMO and LUMO levels. However, the basic features of the electronic structure of the Au_{25} cluster remain unchanged, in clear agreement with the experimental UV−vis results from Figure 13.

CONCLUSIONS

In summary, several homologues of the alkanedithiol series were used for the ligand exchange experiments with the $Au_{25}(SCH_2Ph)_{18}^-$ nanocluster. The extent of exchange reactions, monitored via mass spectrometry, depends on chain length, concentration of the dithiol, and reaction time. A direct energy comparison of the interstaple versus intrastaple binding is made in support of the interstaple binding. Behavior of individual dithiols in such reactions is also verified computationally and presented in parallel to the experimental data. Propanedithiol (C3) and butanedithiol (C4) have optimal chain lengths for interstaple binding onto the nanoparticle surface, achieving more than six interstaple bindings. Pentanedithiol (C5) and hexanedithiol (C6) also participate in these reactions to a lesser extent, while ethanedithiol (C2) does not have optimal chain length for bidentate binding. Moreover, analysis of the S−Au−S angle for the dithiols and formation of the disulfide bond from C2 during exchange indicate that intrastaple binding is likely for C6 or longer dithiols. Further, probing the electronic properties of the postexchange clusters through UV−vis measurements shows the conservation of electronic properties. Efforts will be made in the direction of controlled and complete exchange of such multidentate ligands onto the nanocluster surface.

ASSOCIATED CONTENT

Supporting Information. Additional MALDI-MS and NMR data. Complete ref 55. This material is available free of charge via the Internet at http://pubs.acs.org.

AUTHOR INFORMATION

Corresponding Author
amal@olemiss.edu

Author Contributions
§These authors contributed equally.

ACKNOWLEDGMENT

A.D. gratefully acknowledges support from the National Science Foundation (0903787), University of Mississippi Startup Fund, and CLA summer research grant. G.T. acknowledges NSF (CHE-0957317 and EPS-0903787) and the Mississippi Center for Supercomputing Research. D.L.M. gratefully acknowledges support from the National Science Foundation CHE 0848206. D-E.J was supported by the Division of Chemical Sciences, Geosciences, and Biosciences, Office of Basic Energy Sciences, U.S. Department of Energy. We thank Charles Hussey, Glen Hopkins, and College of Liberal Arts for Bruker Autoflex I MALDI TOF instrumentation support. This research used resources of the National Energy Research Scientific Computing Center, which is supported by the Office of Science of the U.S. Department of Energy under Contract No. DE-AC02-05CH11231.

REFERENCES

(1) Daniel, M.-C.; Astruc, D. *Chem. Rev.* **2003**, *104*, 293–346.
(2) Alivisatos, A. P. *Science* **1996**, *271*, 933–937.

(3) Medintz, I. L.; Uyeda, H. T.; Goldman, E. R.; Mattoussi, H. *Nat. Mater.* **2005**, *4*, 435–446.
(4) Bowman, M. C.; Ballard, T. E.; Ackerson, C. J.; Feldheim, D. L.; Margolis, D. M.; Melander, C. *J. Am. Chem. Soc.* **2008**, *130*, 6896–+.
(5) Penn, S. G.; He, L.; Natan, M. J. *Curr. Opin. Chem. Biol.* **2003**, *7*, 609–615.
(6) Han, G.; Ghosh, P.; Rotello, V. M. *Nanomedicine* **2007**, *2*, 113–123.
(7) Aiken, J. D.; Finke, R. G. *J. Mol. Catal. A: Chem.* **1999**, *145*, 1–44.
(8) Zhu, Y.; Qian, H. F.; Jin, R. C. *Chem.—Eur. J.* **2010**, *16*, 11455–11462.
(9) Schmid, G.; Baumle, M.; Geerkens, M.; Helm, I.; Osemann, C.; Sawitowski, T. *Chem. Soc. Rev.* **1999**, *28*, 179–185.
(10) Brust, M.; Walker, M.; Bethell, D.; Schiffrin, D. J.; Whyman, R. *J. Chem. Soc., Chem. Commun.* **1994**, 801–802.
(11) Whetten, R. L.; Khoury, J. T.; Alvarez, M. M.; Murthy, S.; Vezmar, I.; Wang, Z. L.; Stephens, P. W.; Cleveland, C. L.; Luedtke, W. D.; Landman, U. *Adv. Mater.* **1996**, *8*, 428–433.
(12) Murray, R. W. *Chem. Rev.* **2008**, *108*, 2688–2720.
(13) Jin, R. *Nanoscale* **2010**, *2*, 343–362.
(14) Sardar, R.; Funston, A. M.; Mulvaney, P.; Murray, R. W. *Langmuir* **2009**, *25*, 13840–13851.
(15) Chen, S. W.; Ingram, R. S.; Hostetler, M. J.; Pietron, J. J.; Murray, R. W.; Schaaff, T. G.; Khoury, J. T.; Alvarez, M. M.; Whetten, R. L. *Science* **1998**, *280*, 2098–2101.
(16) Quinn, B. M.; Liljeroth, P.; Ruiz, V.; Laaksonen, T.; Kontturi, K. *J. Am. Chem. Soc.* **2003**, *125*, 6644–6645.
(17) Wyrwas, R. B.; Alvarez, M. M.; Khoury, J. T.; Price, R. C.; Schaaff, T. G.; Whetten, R. L. *Eur. Phys. J. D* **2007**, *43*, 91–95.
(18) Alvarez, M. M.; Khoury, J. T.; Schaaff, T. G.; Shafigullin, M. N.; Vezmar, I.; Whetten, R. L. *J. Phys. Chem. B* **1997**, *101*, 3706–3712.
(19) Shichibu, Y.; Negishi, Y.; Tsunoyama, H.; Kanehara, M.; Teranishi, T.; Tsukuda, T. *Small* **2007**, *3*, 835–839.
(20) Donkers, R. L.; Lee, D.; Murray, R. W. *Langmuir* **2004**, *20*, 1945–1952.
(21) Jimenez, V. L.; Georganopoulou, D. G.; White, R. J.; Harper, A. S.; Mills, A. J.; Lee, D. I.; Murray, R. W. *Langmuir* **2004**, *20*, 6864–6870.
(22) Negishi, Y.; Nobusada, K.; Tsukuda, T. *J. Am. Chem. Soc.* **2005**, *127*, 5261–5270.
(23) Negishi, Y.; Chaki, N. K.; Shichibu, Y.; Whetten, R. L.; Tsukuda, T. *J. Am. Chem. Soc.* **2007**, *129*, 11322–11323.
(24) Wu, Z.; Suhan, J.; Jin, R. *J. Mater. Chem.* **2009**, *19*, 622–626.
(25) Dharmaratne, A. C.; Krick, T.; Dass, A. *J. Am. Chem. Soc.* **2009**, *131*, 13604–13605.
(26) Donkers, R. L.; Lee, D.; Murray, R. W. *Langmuir* **2008**, *24*, 5976–5976.
(27) Love, J. C.; Estroff, L. A.; Kriebel, J. K.; Nuzzo, R. G.; Whitesides, G. M. *Chem. Rev.* **2005**, *105*, 1103–1169.
(28) Ulman, A. *Chem. Rev.* **1996**, *96*, 1533–1554.
(29) Templeton, A. C.; Wuelfing, M. P.; Murray, R. W. *Acc. Chem. Res.* **2000**, *33*, 27–36.
(30) Chinwangso, P.; Jamison, A. C.; Lee, T. R. *Acc. Chem. Res.* **2011**, *44*, 511–519.
(31) Park, J.-S.; Vo, A. N.; Barriet, D.; Shon, Y.-S.; Lee, T. R. *Langmuir* **2005**, *21*, 2902–2911.
(32) Srisombat, L.-o.; Park, J.-S.; Zhang, S.; Lee, T. R. *Langmuir* **2008**, *24*, 7750–7754.
(33) Zhang, S.; Leem, G.; Srisombat, L.-o.; Lee, T. R. *J. Am. Chem. Soc.* **2007**, *130*, 113–120.
(34) Mei, B. C.; Susumu, K.; Medintz, I. L.; Mattoussi, H. *Nat. Protocols* **2009**, *4*, 412–423.
(35) Roux, S.; Garcia, B.; Bridot, J.-L.; Salomé, M.; Marquette, C.; Lemelle, L.; Gillet, P.; Blum, L.; Perriat, P.; Tillement, O. *Langmuir* **2005**, *21*, 2526–2536.
(36) Hou, W.; Dasog, M.; Scott, R. W. J. *Langmuir* **2009**, *25*, 12954–12961.
(37) Zheng, F.; et al. *Nanotechnology* **2008**, *19*, 235603.
(38) Abad, J. M.; Mertens, S. F. L.; Pita, M.; Fernández, V. M.; Schiffrin, D. J. *J. Am. Chem. Soc.* **2005**, *127*, 5689–5694.
(39) Volkert, A. A.; Subramaniam, V.; Ivanov, M. R.; Goodman, A. M.; Haes, A. J. *ACS Nano* **2011**, *5*, 4570–4580.
(40) Stewart, M. H.; Susumu, K.; Mei, B. C.; Medintz, I. L.; Delehanty, J. B.; Blanco-Canosa, J. B.; Dawson, P. E.; Mattoussi, H. *J. Am. Chem. Soc.* **2010**, *132*, 9804–9813.
(41) Tang, Z.; Xu, B.; Wu, B.; Germann, M. W.; Wang, G. *J. Am. Chem. Soc.* **2010**, *132*, 3367–3374.
(42) Tang, Z.; Xu, B.; Wu, B.; Robinson, D. A.; Bokossa, N.; Wang, G. *Langmuir* **2011**, *27*, 2989–2996.
(43) Fields-Zinna, C. A.; Parker, J. F.; Murray, R. W. *J. Am. Chem. Soc.* **2010**, *132*, 17193–17198.
(44) Knoppe, S.; Dharmaratne, A. C.; Schreiner, E.; Dass, A.; Bürgi, T. *J. Am. Chem. Soc.* **2010**, *132*, 16783–16789.
(45) Templeton, A. C.; Hostetler, M. J.; Warmoth, E. K.; Chen, S. W.; Hartshorn, C. M.; Krishnamurthy, V. M.; Forbes, M. D. E.; Murray, R. W. *J. Am. Chem. Soc.* **1998**, *120*, 4845–4849.
(46) Hostetler, M. J.; Templeton, A. C.; Murray, R. W. *Langmuir* **1999**, *15*, 3782–3789.
(47) Dass, A.; Holt, K.; Parker, J. F.; Feldberg, S. W.; Murray, R. W. *J. Phys. Chem. C* **2008**, *112*, 20276–20283.
(48) Shichibu, Y.; Negishi, Y.; Tsukuda, T.; Teranishi, T. *J. Am. Chem. Soc.* **2005**, *127*, 13464–13465.
(49) Chalfant, C. E.; Szulc, Z.; Roddy, P.; Bielawska, A.; Hannun, Y. A. *J. Lipid Res.* **2004**, *45*, 496–506.
(50) Becke, A. D. *Phys. Rev. A* **1988**, *38*, 3098–3100.
(51) Lee, C. T.; Yang, W. T.; Parr, R. G. *Phys. Rev. B* **1988**, *37*, 785–789.
(52) Becke, A. D. *J. Chem. Phys.* **1993**, *98*, 5648–5652.
(53) Clark, T.; Chandrasekhar, J.; Spitznagel, G. W.; Schleyer, P. V. *J. Comput. Chem.* **1983**, *4*, 294–301.
(54) Krishnan, R.; Binkley, J. S.; Seeger, R.; Pople, J. A. *J. Chem. Phys.* **1980**, *72*, 650–654.
(55) Frisch, M. J.; et al. Gaussian 09.
(56) Ahlrichs, R.; Bar, M.; Haser, M.; Horn, H.; Kolmel, C. *Chem. Phys. Lett.* **1989**, *162*, 165–169.
(57) Tao, J. M.; Perdew, J. P.; Staroverov, V. N.; Scuseria, G. E. *Phys. Rev. Lett.* **2003**, *91*, 146401.
(58) Johansson, M. P.; Lechtken, A.; Schooss, D.; Kappes, M. M.; Furche, F. *Phys. Rev. A* **2008**, *77*, 053202.
(59) Weigend, F.; Haser, M.; Patzelt, H.; Ahlrichs, R. *Chem. Phys. Lett.* **1998**, *294*, 143–152.
(60) Andrae, D.; Haussermann, U.; Dolg, M.; Stoll, H.; Preuss, H. *Theor. Chim. Acta* **1990**, *77*, 123–141.
(61) Heaven, M. W.; Dass, A.; White, P. S.; Holt, K. M.; Murray, R. W. *J. Am. Chem. Soc.* **2008**, *130*, 3754–3755.
(62) Zhu, M.; Aikens, C. M.; Hollander, F. J.; Schatz, G. C.; Jin, R. *J. Am. Chem. Soc.* **2008**, *130*, 5883–5885.
(63) Jiang, D. E.; Tiago, M. L.; Luo, W. D.; Dai, S. *J. Am. Chem. Soc.* **2008**, *130*, 2777–2779.

NOTE ADDED AFTER ASAP PUBLICATION

The Supporting Information published ASAP November 22, 2011, did not include the MALDI spectra. The complete Supporting Information was reposted November 29, 2011.